Progress In Electromagnetics Research M, Vol. 68, 31–39, 2018

VLF Monitoring System for Characterizing the Lower Region Ionospheric Layer

Nur A. Zakaria[1, *], Afifah Taat[1], Siti A. E. A. Rahim[1], Wan Z. A. W. Mokhtar[2], and Mohamad H. Jusoh[1]

Abstract—The main objective of the current work is to develop a Very Low Frequency (VLF) monitoring system for characterizing low layer ionosphere. Low layer ionosphere is important for communication, and some researchers stressed that lower layer ionosphere can be a precursor to earthquake event. The VLF monitoring system composed of a 1-m antenna, a preamplifier to amplify the signal, an ADC converter and a data acquisition system. The optimization of 1-m antenna received dual frequencies 19.2 kHz and 19.8 kHz from South Vijayanarayanam, India and North West Cape, Australia, respectively. Subsequently, a low pass filter was designed in the preamplifier to pass VLF signals from 0–30 kHz. The results revealed that the system was able to characterize diurnal variation: sunrise and sunset and detect changes in the lower layer ionosphere region due to Solar activity.

1. INTRODUCTION

Very Low Frequency (VLF; 3–30 kHz) comes from various transmitters around the world and is frequently used in submarines and military communication systems. For example, Naval Communication Station Harold E. Holt is located in North West Cape, Australia. The station delivers VLF radio transmission to United States Navy and Royal Australian Navy ships and submarines in the western Pacific Ocean and Eastern Indian Ocean. The VLF waves are capable to propagate at a very long distance, about 10 to 100 km, and the waves are reflected at lower ionospheric layer (60–95 km). VLF signal efficiently propagates in the space between ground and boundary of the ionosphere. The phenomenon refers to Earth-ionosphere waveguide (EIWG). The propagation characteristics of VLF in EIWG is subject to lower ionospheric ionization, which defines the conductivity profile of the upper boundary of the waveguide. Lower ionospheric ionization process is dependent on solar activities, and undergoes regular and irregular variations. These fluctuations vary the reflected height of VLF signals [1]. Table 1 shows an example of VLF transmitter with call sign, frequency transmitted and the location around the world. Figure 1 illustrates the working principle of VLF monitoring system based on reflection signal at the ionosphere from the transmitter to the receiver.

The ionosphere layers are divided into D-, E-, and F-layer. D-layer is the innermost layer, 60 to 95 km above the surface of the Earth. E-layer extends from 95 to 150 km, and F-layer lies from 160 to over 400 km. Solar Lyman-α radiation at 121.8 nm and EUV radiation at 80 to 11.5 nm are mechanism formation at D-region by ionization of NO, N_2, and O_2 for the duration of daytime.

Solar flares, often referred as sudden, rapid and intense brightness, occur when magnetic energy at solar atmosphere is released. They can be classified according to their strength. A-class is the weakest followed by B, C, M, and X classes. C and B classes have unnoticeable effect on the Earth. M class flares

Received 28 November 2017, Accepted 30 March 2018, Scheduled 27 April 2018

* Corresponding author: Nur Ain Zakaria (nurainzakaria@yahoo.com).

[1] Applied Electromagnetic Research Group (AERG), Faculty of Electrical Engineering, Universiti Teknologi MARA, 40450 Shah Alam, Selangor, Malaysia. [2] Department of Physics, Faculty of Science and Mathematics, Universiti Pendidikan Sultan Idris, 35900 Tanjung Malim, Perak, Malaysia.

Table 1. Example of VLF Transmitter around the world.

Call Sign	Frequency (Hz)	Location
VTX3	18200	South Vijayanarayanam, India
VTX4	19200	South Vijayanarayanam, India
NWC	19800	North West Cape, Australia
HWU	15100 18300 21750 22600	Rosnay, France

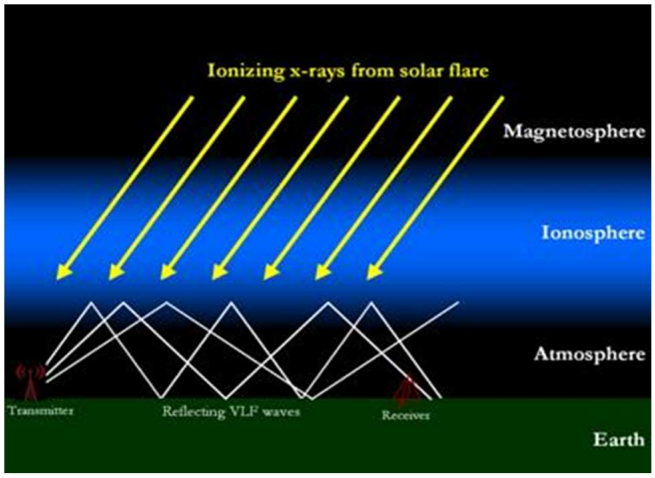

Figure 1. The signal travel very long distance from the transmitter to receiver reflected through the Earth-Ionosphere Wave Guide (EIWG) [5].

can cause brief radio blackouts at the poles and minor radiation storms that might endanger astronauts. Finally, the highest strength of solar flare is X class. It can create long lasting radiation storms that can damage satellite, communications system, ground-based technologies and power grids [2].

The lower D region is unlike the E and F layers, and the free electrons are totally disappeared during nighttime in line to recombination process with oxygen ion to produce neutral oxygen molecules. During daytime, free electrons at D-layer appears due to photoionization process. The D-region electron density profile is characterized by the two Wait's parameters; ionosphere reflection height (H') and exponential sharpness factor (β).

During solar flare events, the excess X-ray emission from the Sun increases photoionization process at the lower ionosphere layer, thus, changes the ionosphere parameters which are ionosphere reflection height (H') and exponential sharpness factor (β) [3]. According to [4], there was a solar flare event class C1.5 on 29th January 2007. By using Long Wave Propagation Compatibility model version 2.0, the result revealed that the reflection height (H') value was reduced by 1.2 km and exponential sharpness factor (β) increased by 0.005 km^{-1}. From the result, it is shown that solar flare event has a significant effect on the low ionospheric region.

The Automated Geophysical Observation (AGO) is an unmanned VLF receiver that works at high geomagnetic latitude. The data are sampled at 2 kHz, and working band frequency is 500 Hz to 16 kHz. The AGO uses 30 Watts to allow the system to operate. Apart from that, the AGO operates at the Antarctic Plateau and requires costly maintenance trips yearly to provide fuel to power the system. This system provides scientific data; however, the system is lack of full VLF broadband data. This gap

leads to a valuable room for improvement. Another example is the Atmospheric Weather Educational System for Observation and Modelling of Electromagnetics (AWESOME) VLF receiver developed by Solar Stanford Center. The antenna uses two orthogonal wire loops to each other and to the ground [6]. The AWESOME system is equipped with a Low Noise Amplifier (LNA), Global Positioning System (GPS) and National Instrument Data Acquisition System (NI-DAQ). The system requires about 200 Watts of power to deploy. Though the AWESOME system is extremely sensitive to receive signals as low as tens of femtotesla with broadband coverage from 300 Hz to 50 kHz [7], the system is limited in its deployment station. Thus, the goal of this paper is to develop a low cost and portable VLF monitoring system or receiver for potential use in characterizing the ionospheric lower layer during solar flare event. The antenna and amplifier are able to capture and amplify VLF frequency signals, particularly the signals from VTX4, India and NWC, Australia, with frequencies 19.2 kHz and 19.8 kHz, respectively. In this paper, we present the first diurnal and solar flare event variations of VLF signal receiver installed at Universiti Pendidikan Sultan Idris (UPSI) (Lat: 3.71′ and Long: 101.53′).

2. SYSTEM DESIGN

2.1. Design of Wire Loop Antenna

The wire loop antenna is induced by magnetic components of electromagnetic waves. Figure 2 presents the antenna structure which is constituted by a 1-m wood frame and copper wire as a medium to convert an electromagnetic wave into voltage. The structure is a loop in 25 turns of 1.4 mm (SWG 17) copper wire. The copper wire is used instead of ferrite core loops due to better linearity and to reduce temperature dependence.

Figure 2. Proposed 1-m antenna structures, loop with 25 turns copper wire.

To calculate the impedance, response, and sensitivity of the antenna, the formula can be expressed as [7]:

$$\text{Antenna Turn Length} = c_1\sqrt{A_a} \tag{1}$$

where A_a is the area of antenna, and C_1 is a geometry-related constant of the square antenna with value 4.000.

Next, the antenna turn length is used to find the resistance as follows:

$$R_a = \frac{4\rho N_a c_1\sqrt{A_a}}{\pi d^2} \tag{2}$$

where, resistivity copper $\rho = 1.72 \times 10^{-8}\,\Omega$, N_a is the number of turns, and d is the diameter of the wire.

For the inductance of loop antenna, the formula is given by:

$$L_a = 2.00 \times 10^{-7} N_a^2 c_1 \sqrt{A_a} \left[\ln \frac{c_1 \sqrt{A_a}}{\sqrt{N_a} d} - c_2 \right] \tag{3}$$

C_2 is a geometry-related constant of the square antenna with value 1.217 correspondingly.

The resistance, R_a, and impedance, L_a, will lead to forming an impedance

$$Z_a = R_a + j\omega L_a \tag{4}$$

Due to change in times, as part of the AC cycle, the resistance, R_a, and impedance, L_a, are out of phase. Thus, their peaks are at different times. When the magnetic field of the electromagnetic wave passes the antenna, the voltage will be induced in the loop. The output voltage can be calculated using Faraday's Law [8]

$$V_a = j2\pi f N_a A_a B \cos\theta \tag{5}$$

where V_a is the output voltage, f the frequency signal, B the magnetic flux density (T), and θ the angle of the magnetic field from the axis of the loop.

The antenna sensitivity can be obtained as follows:

$$S_a = \frac{\sqrt{4kTR_a}}{2\pi f N_a A_a} \tag{6}$$

where k is the Boltzmann's constant, and T is the temperature in Kelvins.

To avoid electromagnetic interference and resonance, the antenna needs to be placed in a distant from the places of the generator, electrical equipment and power lines.

2.2. Design of Preamplifier Circuit

The preamplifier was designed by using a BC548 amplifier transistor and TL082CP JFET-Input Operational Amplifiers. The TL082CP Op-Amp have high slew rates and low input bias. The schematic design of the proposed pre-amplifier for VLF monitoring system using the mentioned components is shown in Figure 3 and Figure 4. The preamplifier employs *CE* configuration for the first stage, in which the base and emitter terminals constitute the input port, and the collector-emitter terminals are the output. *CE* configuration has greater efficiency in increasing voltage and current of AC signal than *CB* and *CC* configurations. A C_1 is implemented to block direct current that may be present in the circuit and allows only AC voltage to the transistor. Correspondingly, C_4 is a blocking capacitor, on condition of dc isolation between the amplifier and the Op-amp [9].

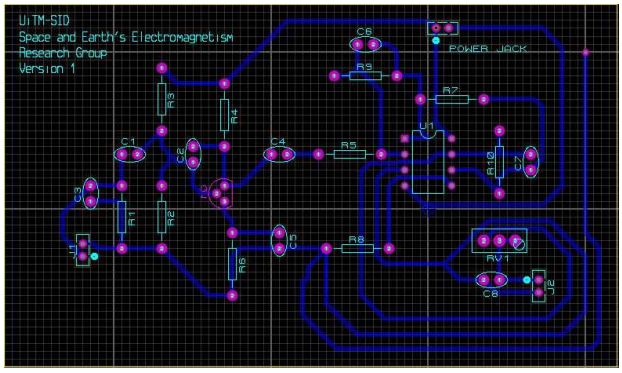

Figure 3. The layout diagram of the printed circuit board and its component placement.

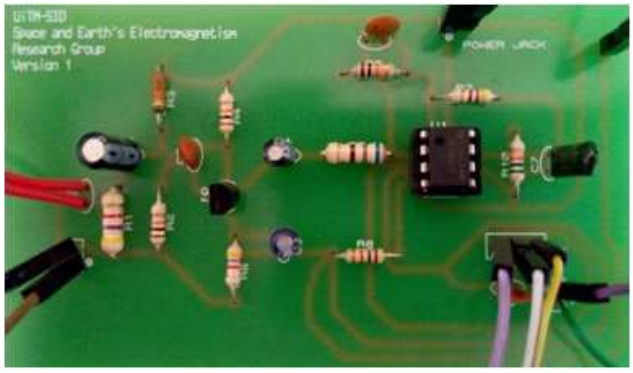

Figure 4. The preamplifier circuit with components.

3. MEASUREMENT

The measurement was carried out using a signal generator, spectrum analyzer, and an oscilloscope to measure the sensitivity of the preamplifier. Figure 5 shows the result of the output voltage of preamplifier. The flat frequency response is from 0 to 16 kHz corresponding to gain 24 dB. However, the amplifier still works until 30 kHz with gain 18 dB.

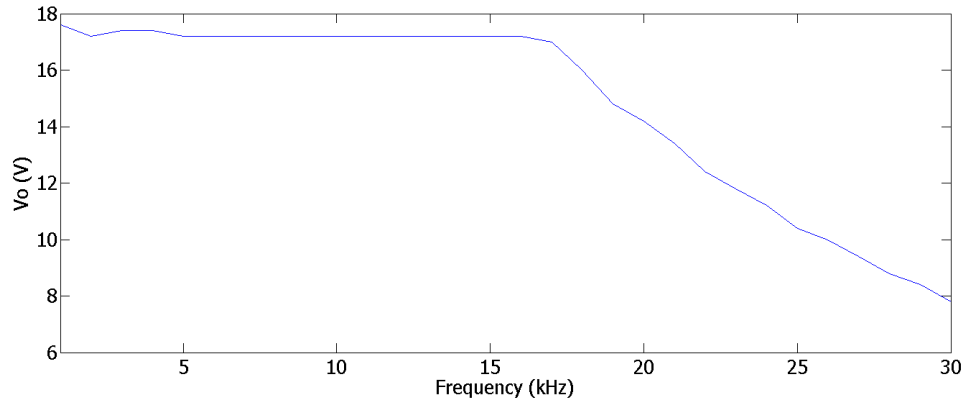

Figure 5. The output voltage preamplifier was tested from 0 to 30 kHz.

In view of the spectrum analyzer results obtained in Figure 6, power spectral density at the frequency 19.8 kHz is −42.9 Hz/dBm. The spectrum analyzer measures magnitude of the input signal with 10 kHz span. The results indicate that the wire loop antenna is capable to work at 19.8 kHz.

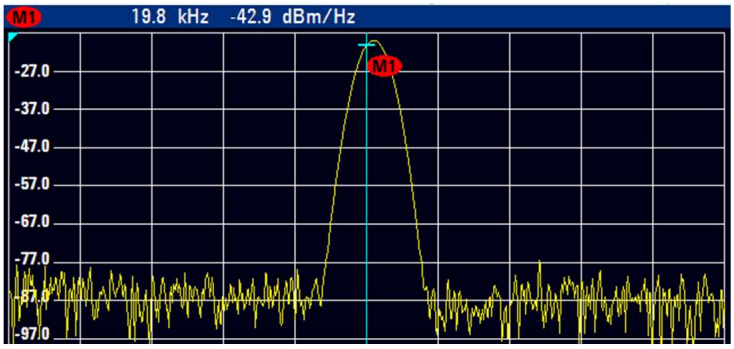

Figure 6. Spectrum analyzer detects signal 19.8 kHz with −42.9 dBm/Hz power spectral density.

3.1. Radiation Pattern in the Lab

Figure 7 shows the result of E-plane pattern tested in the lab. As can be seen, Figures 7(a) and 7(b) show the result of 1-m magnetic loop antenna pattern at frequency 19.2 kHz and 19.8 kHz tested in the lab without interference from the signal outside. The result shows a good bidirectional pattern. The working angles for the two frequencies, 19.2 kHz and 19.8 kHz, are 120° to 230° and 70° to 300°. The working angle of the antenna can be explained by the angle between the coil plane and the propagation direction of the Electromagnetic (EM) wave as depicted in Figure 7(c). When the propagation direction of the EM wave is parallel to the coil plane at $\phi = 0°$ or $\phi = 180°$, the induced voltage of the magnetic antenna is maximum, and it will show the peak in the magnetic pattern. When the propagation direction of EM wave is vertical to the coil plane for example angle at $\phi = 90°$ or $\phi = 270°$, the induced voltage of the magnetic antenna is minimum, which is the zero in the magnetic pattern. The results are in

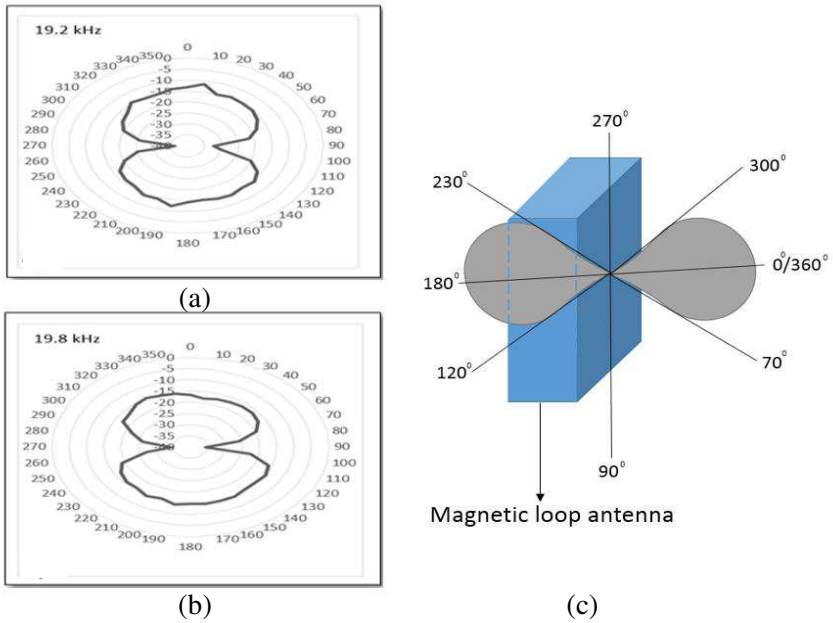

Figure 7. Radiation pattern of 1-m magnetic loop antenna tested in the lab at the frequency 19.2 kHz and 19.8 kHz.

agreement that 1-m magnetic loop antenna works for the corresponding frequency and is able to work when the parallel signal is induced at the angle $\phi = 0°$ or $\phi = 180°$.

3.2. Radiation Pattern at the Installation Site

Figures 8(a) and 8(b) present the result of 1-m magnetic loop antenna directional pattern tested at the installation site UPSI. The antenna is used to capture two frequencies at a time. The antenna is directed to North West Cape, Australia that transmits the frequency signal 19.8 kHz. At the same time, the antenna is also able to receive frequency 19.2 kHz from South Vijayanarayanam, India. The antenna is able to receive 19.2 kHz signal from $\phi = 40°$ to $\phi = 310°$ and $\phi = 150°$ to $\phi = 210°$. For the signal 19.8 kHz, the working angles for the antenna are $\phi = 10°$ to $\phi = 100°$ and $\phi = 160°$ to $\phi = 280°$. Figure 8(c) illustrate the combination angle of working frequency for both signals. The cross-sectional angle of the magnetic loop antenna proves that the ability of the antenna to capture signal 19.2 kHz from India is decreased due to the antenna directed statically at the Australia that transmitted signal 19.8 kHz. The results are in agreement with the plotted data in the next section. The data from Australia demonstrate a good variation compared to the data from India.

4. DATA VALIDATION

Figure 9 shows a map of the path between the transmitter station and receiver station. Receiver station at UPSI receives dual frequencies at a time. To validate and verify the new station data, data from another established station in Malaysia are taken for analysis. Data from another station are denoted as UKM_NWC. The receiver station is at Universiti Kebangsaan Malaysia (UKM) and the transmitter station at NWC, Australia.

4.1. Diurnal Variation

The key aspect to confirm the VLF monitoring system is working properly by monitoring the diurnal variation of the system. Refer to Figures 10(a) and (c) shows the data captured by VLF monitoring system located at UPSI, and Figure 10(b) shows the data captured by VLF monitoring system located

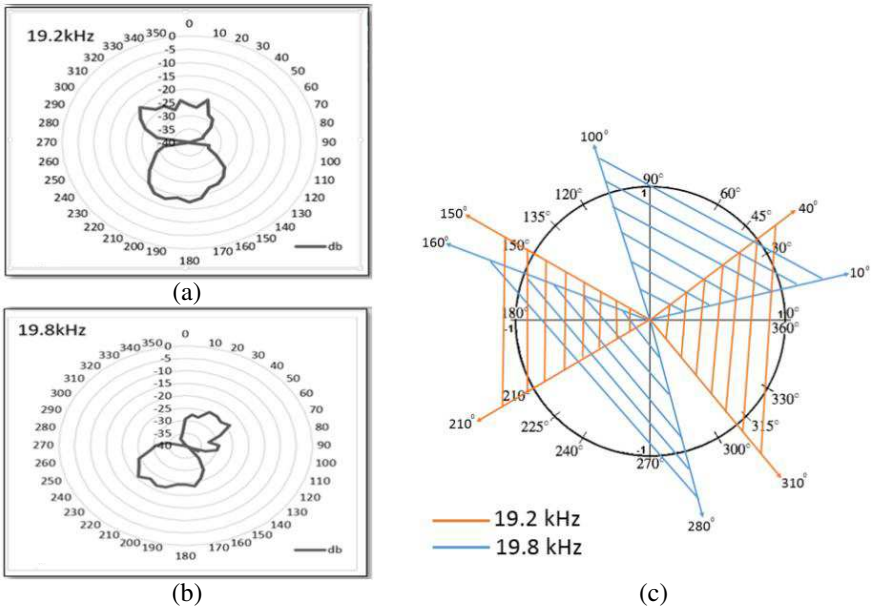

Figure 8. Radiation pattern of 1-m magnetic loop antenna tested at the installation site.

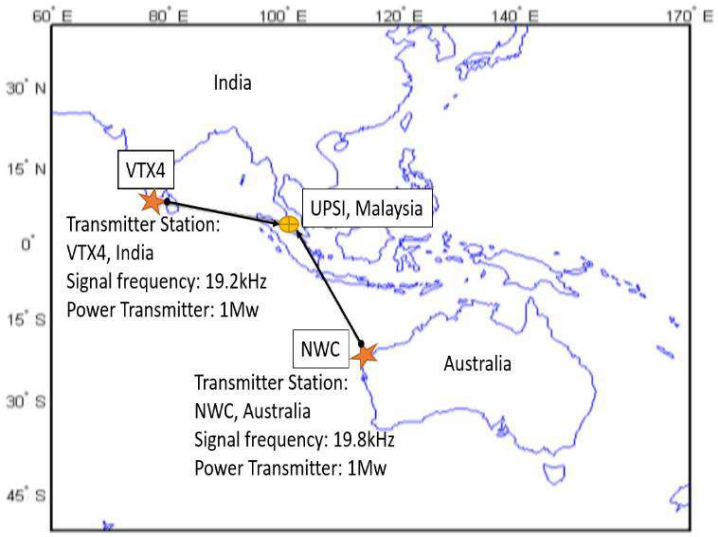

Figure 9. A map of transmitted VLF navigation signal from VTX4, India and NWC, Australia over a great circle path of 2694 km and 3111 km respectively.

at UKM. The patterns of the two receiver stations are similar. At sunrise from 0530 to 0730 local time, the readings for both stations decrease sharply. It is the same phenomena happening during sunset. The decreasing reading during sunrise and sunset is called terminator time (TT). It is a time when the terminator line crosses given locations along the VLF propagation path creating amplitude minima at the receiver [10]. It is also defined as the time of amplitude minimum that coincides very well with the time of maximum rate of phase change [11]. Apart from that, the average value of signal strength from 0600 to 1800 local time (period for hunting solar flare) when there is no event from Sun is 70 dB.

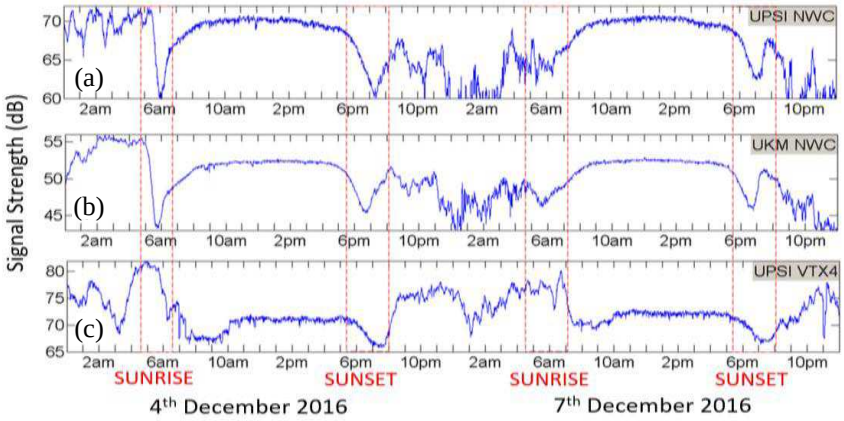

Figure 10. Diurnal amplitude variation received at UPSI and UKM stations.

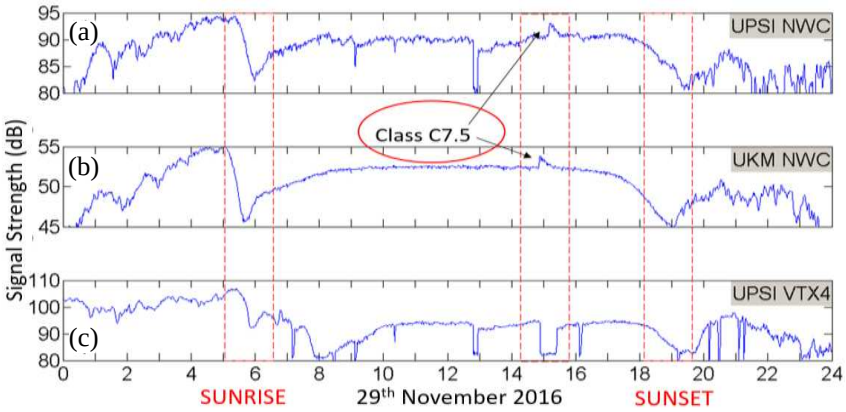

Figure 11. Detection of solar flare class C7.5 at 3.03pm local time.

4.2. Detection of a Solar Flare

In preference to diurnal fluctuations, activities on the Sun can effect sudden changes to the ionosphere. Referred to Figure 11, there is a sudden impulse in the value of signal strength at 15.03 local time. This is a clear evidence when the height of the reflection of the VLF waves decreases due to solar flare activity, resulting in considerable decrease separation between the walls of EIWG. When the energy of solar flares reaches the Earth's upper atmosphere, the ionization in the ionosphere increases suddenly. As a consequence of this separation, the value of signal strength is high at the receiver as depicted in Figure 11. The occurrence of solar flare event was detected by UPSI and UKM stations with the class of C7.5. The peak changes occurring in the ionosphere can be termed as Sudden Ionospheric Disturbance (SID). The ionosphere takes a few seconds to several minutes to recover itself to normal conditions.

5. CONCLUDING REMARKS

After the studies were done, it was remarked that the data achieved were in good conformity with the established system at UKM, and the solar flare event was validated by the report from U.S. Department of Commerce, NOAA, Space Weather Prediction Center. The data extracted from this system can be used to characterize the lower layer ionosphere mainly D- and E-regions with heights 60 to 95 km and 95 to 150 km, respectively. The characterization parameters can be developed by considering three main conditions which are quiet, a disturbing period of space weather and signal strength value of TT.

ACKNOWLEDGMENT

The authors acknowledge Stanford Solar Center, Space Science Centre, UKM, Universiti Pendidikan Sultan Idris (UPSI), and University Malaya (UM) for providing technical support, data, and location. Besides, highest gratitude sent to Universiti Teknologi MARA for the management support and consideration throughout this project. This research financially supported by Fundamental Research Grant Scheme, FRGS (Code No. 600-RMI/FRGS 5/3 140/2014).

REFERENCES

1. Indira Devi, M., I. Khan, and D. N. Madhusudhana Rao, "A study of VLF wave propagation characteristics in the earth-ionosphere waveguide," *Earth Planet and Space*, Vol. 60, 737–741, Jul. 2008.
2. Contreira, D. B., F. S. Rodrigues, K. Makita, et al, "An experiment to study solar flare effects on radio-communication signals," *Advances in Space Research*, Vol. 36, 2455–2459, Mar. 2004
3. Abd Rashid, M. M., M. Ismail, A. M. Hasbie, and R. Nordin, "Ionospheric disturbances triggered by solar flare events during solar maximum — May 2013," *2015 IEEE 12th Malaysia International Conference on Communications (MICC)*, Malaysia, 2015.
4. Kumar, A. and S. Kumar, "Space weather effects on the low latitude D-region ionosphere during solar minimum," *Earth, Planets and Space*, 66–76, 2014.
5. "The Earth's Ionosphere", [Online], Available: http://solar-center.stanford.edu/SID/activities/ionosphere.html, Accessed: Nov. 28, 2017.
6. Cohen, M. B., U. S. Inan, and E. W. Paschal., "Sensitive broadband ELF/VLF radio reception with the AWESOME instrument," *IEEE Transaction on Geoscience and Remote Sensing*, 1–15, 2009.
7. Harriman, S. K., W. Paschal, and U. S. Inan. "Magnetic sensor design for femtotesla low-frequency signals," *IEEE Transaction on Geoscience and Remote Sensing*, Vol. 48, 396–402, 2010.
8. Tan, L. M., "Development of TNU-SuperSID teaching module for observing the effects of solar activities on the lower ionosphere," *Journal of Physical Science and Application*, Vol. 5, 116–122, 2015.
9. Holt, C. A., "Basic amplifier configuration," *Electronic Circuits Digital and Analog*, 383–389, John Wiley & Sons, Canada, 1978.
10. Samanes, J. E., J. P. Raulin, and E. L. Macotela, "Estimating the VLF modal interference distance using The South America VLF network (SAVNET)," *Radio Science*, Vol. 50, 122–129, Feb. 2015.
11. Muraoka, Y., "A new approach to mode conversion effects observed in a mid-latitude VLF transmission," *Journal of Atmospheric and Terrestrial Physics*, Vol. 44, 855–862, Oct. 1982.